*Korean J. Chem. Eng.*, **28**(3), 717-722 (2011)
DOI: 10.1007/s11814-010-0424-z

# Preparation of well-dispersed and anti-oxidized Ni nanoparticles using polyamioloamine dendrimers as templates and their catalytic activity in the hydrogenation of *p*-nitrophenol to *p*-aminophenol

**Zhenye Ma*,**,†, Rujun Wu*, Qiaorong Han*, Rizhi Chen**, and Zhenggui Gu***

*College of Chemistry and Material Science, Nanjing Normal University, Nanjing, Jiangsu 210097, China
**State Key Laboratory of Materials-Oriented Chemical Engineering; College of Chemistry and Chemical Engineering, Nanjing University of Technology, Nanjing 210009, China
(*Received 18 July 2010 • accepted 6 September 2010*)

**Abstract**−*p*-Aminophenol was synthesized by catalytic hydrogenation of *p*-nitrophenol on Ni nanoparticles prepared by a chemical reduction method using polyamidoamine (PAMAM) dendrimers as templates. The as-prepared Ni nanoparticles were characterized by XRD, LRS, EDS, FTIR, FESEM, HRTEM and $N_2$ sorption analysis. Smaller-sized, better-dispersed and more active Ni nanoparticles can be successfully achieved using PAMAM dendrimers as templates. Analysis results show the as-prepared Ni nanoparticles are pure f.c.c. nickel. In hydrogenation reactions of *p*-nitrophenol, Ni nanoparticles show higher catalytic activity than that of Ni nanoparticles prepared in the absence of PAMAM dendrimers. The weight ratio of PAMAM/$Ni^{2+}$ is proved to be an important parameter on the catalytic activity of Ni nanoparticles and the optimal ratio is 15%. The reason proposed for higher catalytic activity of Ni nanoparticles is a combination effect of smaller particle size, better dispersion and more active Ni nanoparticles.

Key words: Ni Nanoparticles, PAMAM Dendrimers, Hydrogenation, *p*-Nitrophenol, Catalytic Activity

## INTRODUCTION

*p*-Aminophenol (PAP) is an important intermediate for the manufacture of analgesic and antipyretic drugs such as paracetamol, acetanilide, phenacetin, and so forth [1-4]. The direct catalytic hydrogenation of *p*-nitrophenol (PNP) is considered as an efficient and green route for the synthesis of PAP [4]. Many catalysts including Raney Ni [5], Ni nanoparticles [6-9], Pd/C [4] and Pd-B/$TiO_2$ [10] have been reported in the synthesis of PAP. Among these catalysts, Ni nanoparticles have received increasing attention as low-cost, high-efficiency and high-selectivity hydrogenation catalysts [5,6]. However, more active surface atoms and smaller size of Ni nanoparticles often bring aggregation and oxidation, which will lead to the decrease in catalytic activity and selectivity.

To avoid aggregation and oxidation of the Ni nanoparticles, various stabilizing methods have been developed and many organic solvents and modifiers such as ethanol [11], tetrahydrofuran [12], hexadecylamine [13] and thylene glycol [14] have been used. Unfortunately, the strong absorption of these stabilizers on the active sites of the Ni nanoparticles often results in the loss of catalytic activity and selectivity. Recently, Wang et al. [15] reported the effect of organic modifiers on the structure and catalytic activity of Ni nanoparticles in the liquid hydrogenation of *p*-nitrophenol. Although the phase-pure metallic Ni can be successfully achieved, the aggregation of Ni nanoparticles is still severe and the catalytic activity needs to be further improved.

Polyamidoamine (PAMAM) dendrimers are perfect candidates for their relatively well-defined shape, narrow molecular weight distribution and high density of amino groups at their periphery. It is well-known for various applications ranging from forming drug delivery systems [16,17], to forming nanoparticle templates [18-21], to forming adhesion materials for high quality metal film formation [22,23]. By utilizing the PAMAM dendrimers as templates, it is favorable to obtain well-dispersed and anti-oxidized Ni nanoparticles. Crooks and co-workers [24] have reported the synthesis of sixth-generation PAMAM dendrimers stabilized Ni nanoparticles. However, to the best of our knowledge, these PAMAM dendrimers stabilized Ni nanoparticles have not yet been used in the hydrogenation of *p*-nitrophenol to *p*-aminophenol.

Herein, we report the preparation of Ni nanoparticles using amine-terminated 2-generation PAMAM dendrimers as templates by a chemical reduction method. The structures of the as-prepared Ni nanoparticles were characterized by XRD, LRS, FTIR, EDS, FESEM HRTEM and $N_2$ sorption analysis. PAP was synthesized by catalytic hydrogenation of p-nitrophenol on Ni nanoparticles. The results show that well-dispersed and anti-oxidized Ni nanoparticles were achieved. The as-prepared Ni nanoparticles exhibit higher catalytic activity compare to the Ni nanoparticles prepared in the absence of PAMAM dendrimers.

## EXPERIMENTAL

### 1. Catalyst Preparation

$NiSO_4 \cdot 6H_2O$ and $N_2H_4 \cdot H_2O$ were purchased from Aldrich. All reagents were used without further purification.

Amine-terminated generation 2 PAMAM dendrimers were synthesized and purified according to the literature procedures [25].

The preparation method of Ni nanoparticles using PAMAM dendrimers as templates is as follows. A solution of nickel ion was first

†To whom correspondence should be addressed.
E-mail: mzynjust@163.com

prepared by dissolving $NiSO_4 \cdot 6H_2O$ (0.25 mol/L, 50 ml) with distilled water in the dissolving tank equipped with a temperature-control system and an agitator. Then PAMAM dendrimers (0.01 g/ml, 4.9 ml) were added and agitated for 0.5 h at 80 °C. $N_2H_4 \cdot H_2O$ (0.1 M, 15 ml) in NaOH (0.1 M) solution was then added. The reaction mixture was stirred until no significant bubbles were observed. Then the resulting suspension was washed thoroughly with distilled water and subsequently with 99.9% alcohol (EtOH). The as-prepared Ni nanoparticles were marked with Ni (A).

For comparison, pure Ni nanoparticles were also prepared according to above method without addition of PAMAM and the as-prepared Ni nanoparticles were marked with Ni (B).

**2. Catalyst Characterization**

X-ray diffraction (XRD) was performed on a Bruker D8 Advance instrument using Cu K$\alpha$ radiation ($\lambda$=0.154178 nm) from 20° to 80° (in 2$\theta$) with the scanning rate of 3°/min. Field-emission scanning electron micrography (FESEM) and energy dispersive spectroscopy (EDS) were obtained on a LEO 1530 VP scanning electron microscope. Fourier transform infrared spectra (FTIR) were obtained using a Shimadzu FTIR-8400s spectrometer equipped with a Specac Silver Gate (ZnSe crystal) single reflection attenuated total reflectance (ATR) system. Spectra were recorded from 450 to 4,000 $cm^{-1}$ using a resolution of 4 $cm^{-1}$ and 150 scans. Laser Raman spectroscopy (LRS) was run on a Labram HR800 Raman Microscope. High resolution transmission electron microscope (HRTEM) images and the corresponding selected-area electron diffraction (SAED) were taken on a JTOL TEM-2100 electron microscope. The Brunauer-Emmett-Teller (BET) surface areas were measured on a Bechman Coulter SA3100 Plus instrument using $N_2$ adsorption at −196 °C.

**3. Catalytic Hydrogenation of PNP**

A simplified schematic diagram of hydrogenation of *p*-nitrophenol is shown in Scheme 1.

The catalytic hydrogenation of *p*-nitrophenol to *p*-aminophenol was performed in a 300 ml stainless steel autoclave with electromagnetic stirrer and temperature control unit. The operation conditions of catalytic *p*-nitrophenol reduction are listed in Table 1. The reactor was heated to a desired temperature under slow stirring (100 rpm). After the temperature equilibrated at the set point, hydrogen gas was introduced to a set pressure and the system was stirred vigorously (300 rpm). At the end of the reaction, the reactor was cooled to the ambient temperature and samples were taken from the reaction system. The solid catalysts were immediately separated from the aqueous phase by centrifugation and the remaining top solution was analyzed by an HPLC (Agilent 1100 Series, USA) equipped with a diode array detector (DAD) and an auto-sampler.

In this paper, the catalytic activity of Ni nanoparticles is expressed by reaction rate defined as the amount of hydrogen consumed per minute and per gram of catalysts.

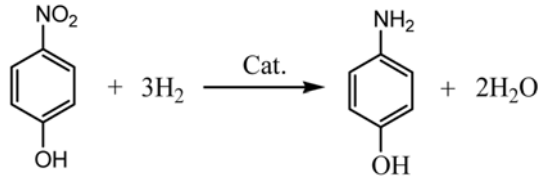


**Scheme 1. Catalytic hydrogenation of *p*-nitrophenol to *p*-aminophenol.**

**Table 1. The operation conditions of catalytic hydrogenation of *p*-nitrophenol**

| Operation conditions | |
|---|---|
| Reaction temperature (K) | 383 |
| Operating pressure (Bar) | 16.5 |
| Volume of ethanol (ml) | 143 |
| Volume of water (ml) | 20 |
| Amount of *p*-nitrophenol (g) | 14 |
| Amount of catalyst (g) | 0.3 |
| Stirring rate (rpm) | 250 |

## RESULTS AND DISCUSSION

**1. Catalyst Characterization**

Fig. 1 shows the XRD patterns of Ni (A) and Ni (B), respectively. The reflection peaks at 44.58°, 51.88° and 76.48° are assigned

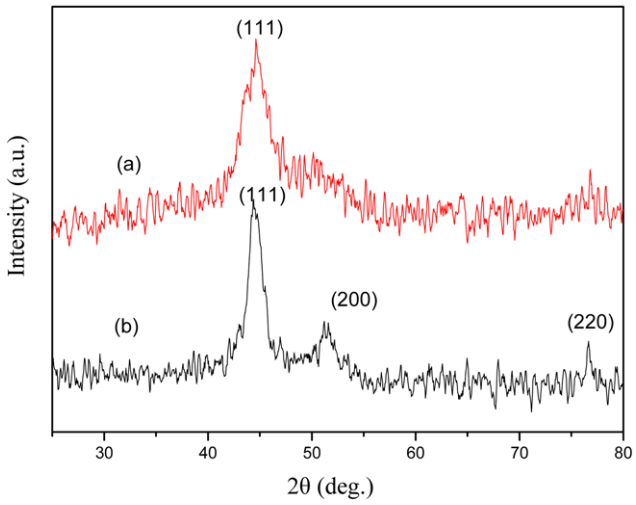


**Fig. 1. XRD patterns of (a) Ni (A) and (b) Ni (B).**

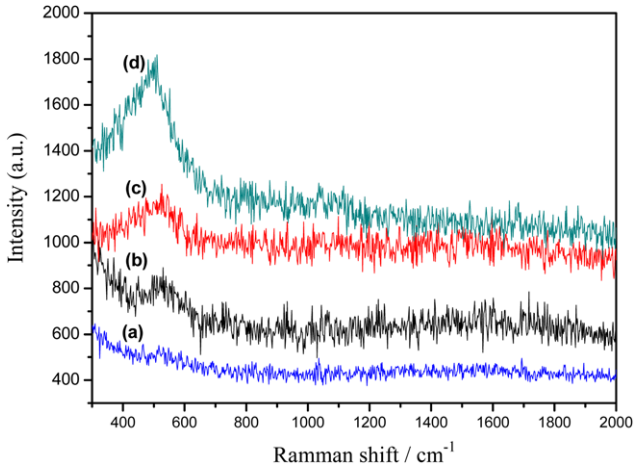


**Fig. 2. LRS of samples (a) Ni (A); (b) Ni (B); (c) Ni (A) stored for 1 year; (d) Ni (B) stored for 1 year.**

to the (1 1 1), (2 0 0) and (2 2 0) crystal planes of Ni metal. They are well-consistent with the JCPDS file (No.04-0850), indicating the formation of Ni metal. No diffraction peaks of NiO and $Ni(OH)_2$ are detected, which may be caused by low concentration. Compared with the reflection peak of Ni (B), the broadening diffraction peak of Ni (A) at 44.58° indicates the presence of relatively smaller particles. The crystalline sizes of nickel crystallite are estimated to be 5 nm for Ni (A) and 8 nm for Ni (B) according to scherrer equation. It is clear that the crystalline size of Ni (A) is smaller than that of Ni (B).

To further confirm the composition and oxidation degree of Ni (A) and Ni (B), LRS is used and the results are shown in Fig. 2. The band at 500 $cm^{-1}$ is assigned to the LRS spectrum of NiO [26], which indicates that some Ni nanoparticles are oxidized in both Ni (A) and Ni (B). The peak intensity of NiO in Ni (A) at 500 $cm^{-1}$ is obviously lower than that in Ni (B), which shows that less Ni nanoparticles are oxidized in Ni (A). EDS also show the same results. The NiO concentration is below the detection limit of XRD, so NiO cannot be detected by XRD. From Fig. 2(c) and Fig. 2(d), it can be seen that the oxidation degree of Ni (B) is still stronger than that of Ni (A) after one year stored. These results mean that the PAMAM dendrimers play an important role to prevent Ni nanoparticles from oxidation in air.

To investigate the action of PAMAM dendrimers, the FTIR of Ni (A) and Ni (B) were measured. Fig. 3 shows the FTIR spectra of Ni (A) and Ni (B) after the baseline calibration (with thermo nicolet FTIR software omnic 5.0). The inset gives the original FTIR spectra of Ni (A) and Ni (B). As shown in the inset, nearly no difference of FTIR spectrum of Ni (A) and Ni (B) can be observed. This may be caused by the low concentration of PAMAM dendrimers in Ni (A), which is below the detection limit of FTIR. However, the FTIR spectra of Ni (A) and Ni (B) after the baseline calibration are obviously different. For Ni (A), the two absorption bands appearing at 2,923 and 2,852 $cm^{-1}$ result from the C-H asymmetric and symmetric stretching vibration, while the peak at 1,390 $cm^{-1}$ corresponds to the C-H

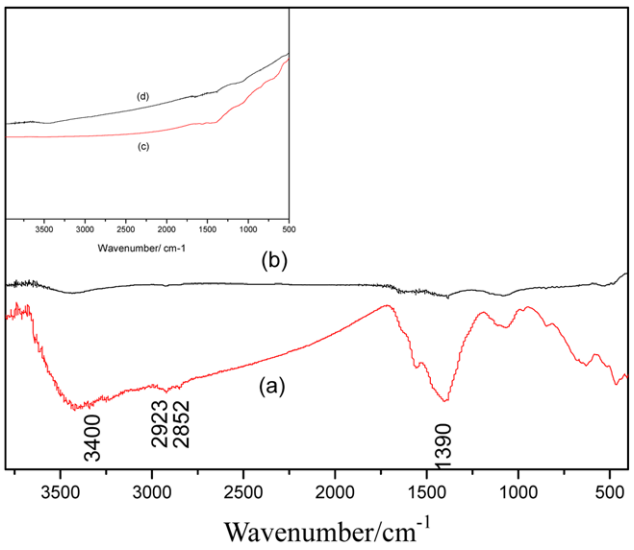


**Fig. 3. FTIR spectra of (a) Ni (A) and (b) Ni (B) after the baseline calibration. The inset gives the original FTIR spectra of (c) Ni (A) and (d) Ni (B).**

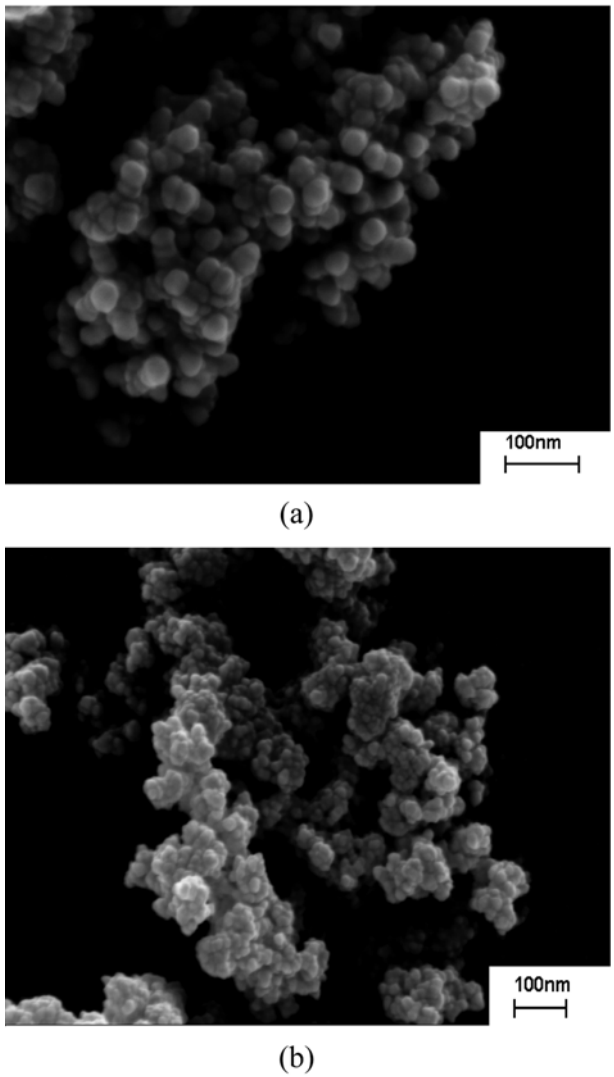


**Fig. 4. FESEM images of (a) Ni (A) and (b) Ni (B).**

deformation in the methylene ($-CH_2$) groups. The result shows that there are still minimum PAMAM dendrimers on the surface of Ni nanoparticles. The coating of PAMAM dendrimers on the surface of Ni (A) prevents the oxidation of Ni nanoparticles in air.

The size, shape and dispersion of Ni (A) and Ni (B) can be characterized with FESEM and HRSEM. The typical FESEM images are shown in Fig. 4. It is clear that the Ni (A) is spherical with the size of 20 nm or so. The dispersion of two kinds of Ni nanoparticles is distinctly different. Compared to Ni (B), Ni (A) exhibits better dispersion and the single Ni nanoparticles can be seen clearly. The HRTEM image (Fig. 5(a)) also shows the better dispersion of Ni (A). The lattice fringes of the Ni (A) shown in Fig. 5(b) are examined to be 0.202 and 0.179 nm, corresponding to the (111) and (200) lattice spacing of the fcc nickel, respectively. The SAED patterns (inset in Fig. 5(a)) show that the primary nickel nanoparticles have polycrystalline structures.

The above results show smaller-sized, better-dispersed and more active Ni nanoparticles can be successfully achieved using amine-terminated generation 2 PAMAM dendrimers as templates. This may be attributed to the action of PAMAM dendrimers. It is reported

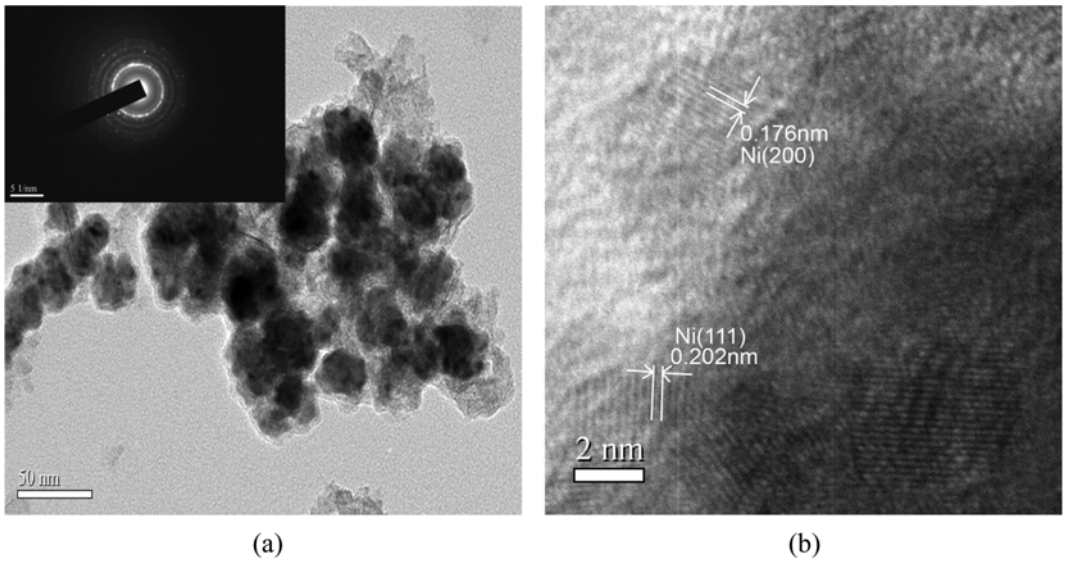


**Fig. 5. Low- and high-resolution HRTEM images of the Ni(A). The inset shows the corresponding SAED patterns, and the diffraction rings are assigned to (111), (200), (220), and (311) reflections of fcc nickel metal.**

PAMAM dendrimers can provide a unique microenvironment, making them interesting candidates for host-guest chemistry [27]. In our research, PAMAM dendrimers have been used as nanoscale templates in the synthesis and stabilization of Ni nanoparticles. First, metal nickel ions pass through the gap of PAMAM macromolecules and enter into inner of the PAMAM macromolecules in the aqueous solution. Then, the dendrimer macromolecules that have numerous reactive functional groups as hosts to complex with metal nickel ions. At last, the metal nickel ions immobilized by the PAMAM dendrimers are reduced by the $N_2H_4$• $H_2O$ to form Ni nanoparticles. The adsorption and complexation of PAMAM dendrimers prevent the growth and aggregation of Ni nucleus, which is in favor of the formation of smaller-sized and better-dispersed Ni nanoparticles. The existence of minim PAMAM dendrimers on the surface of Ni nanoparticles can prevent the oxidation of Ni nanoparticles in air.

## 2. Catalytic Activity

The catalytic properties of the Ni nanoparticles were investigated in the hydrogenation of *p*-nitrophenol to *p*-aminophenol. The results are illustrated in Fig. 6. For Ni (B), the hydrogenation rate first increases with time and then stabilizes with respect to the *p*-nitrophenol hydrogenation. The first stage corresponds to the activation of Ni nanoparticles because of the existence of NiO. Therefore, during the hydrogenation, these NiO are first reduced by hydrogen to nickel, resulting in increasing the effective amount of nickel and the catalytic activity. The second stage is related to the concentration of *p*-nitrophenol, namely, that the hydrogenation rate is not affected by *p*-nitrophenol concentration except at lower concentrations [5]. It is interesting that the activation stage doesn't nearly exist for Ni (A), which may be caused by the less NiO amount. The hydrogenation rate of Ni (A) is clearly higher than that of Ni (B) at similar reaction conditions, which shows that Ni (A) exhibits better catalytic activity than that of Ni (B). From the foregoing results of catalyst characterization, we suggest that the reason for higher catalytic activ-

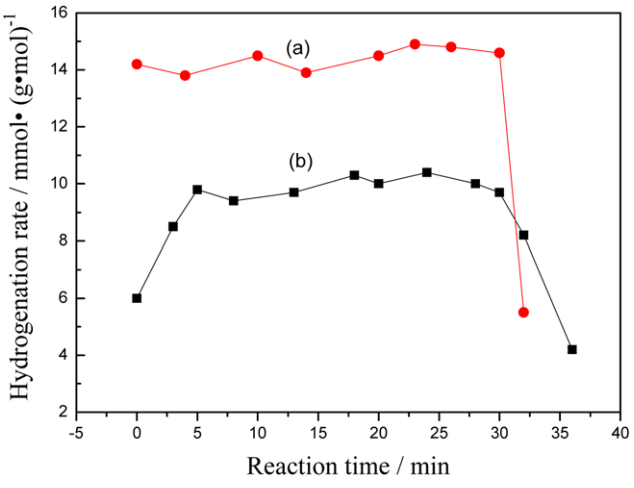


**Fig. 6. Reaction rate of *p*-nitrophenol hydrogenation with (a) Ni (A) and (b) Ni (B).**

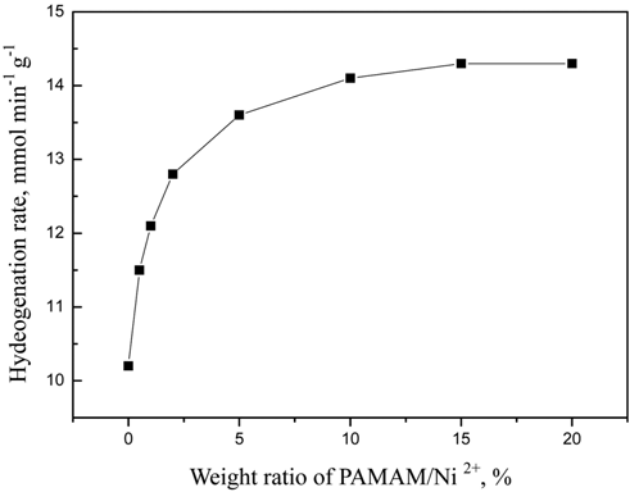


**Fig. 7. Effect of weight ratio of PAMAM to Ni on the catalytic activity of Ni (A).**

**Table 2. The BET results of different catalysts**

| Weight ratio of PAMAM to Ni | BET ($m^2g^{-1}$) |
|---|---|
| 0% | 16.50 |
| 0.5% | 17.26 |
| 1% | 17.88 |
| 2% | 18.25 |
| 5% | 18.85 |
| 10% | 19.53 |
| 15% | 19.72 |

ity of Ni (A) is a combination effect of the smaller size, more active Ni and better dispersion. At the same time, the product of hydrogenation reaction was analyzed by HPLC. *p*-Aminophenol is found to be the only product for Ni (A) and Ni (B), implying that the selectivity is almost 100%.

In addition, the effect of the weight ratio of PAMAM to Ni on catalytic activity of Ni (A) was also investigated and the results are shown in Fig. 7 (the catalytic activity is expressed as the reaction rate at 20 min). It is seen that the activity of Ni (A) catalyst changes with the increase of the weight ratio of PAMAM to Ni at three different stages. The activity increases sharply with the increase of the weight ratio of PAMAM to Ni from 0.5 wt% to 2 wt% and increases slowly with the increase of the weight ratio of PAMAM to Ni from 2 wt% to 15 wt%. The activity remains nearly constant with further increase of Ni loading from 15 wt% to 20 wt%.

The complexation of PAMAM with metal ions plays an important role in the dendrimer stabilized nanoparticles. The results of BET surface areas of different catalysts are listed in Table 2. It can be seen that BET surface area of different catalysts increases with the increase of the weight ratio of PAMAM to Ni, which shows that the PAMAM dendrimers can improve the dispersion of the Ni nanoparticles. Higher PAMAM dendrimer concentration increases the ability to complex with metal nickel ions and to stabilize nanoparticles synchronously. When the complexation reaches saturation condition, further increasing the PAMAM concentration has no observable effect on the stability of the Ni nanoparticles.

## CONCLUSIONS

We have demonstrated the formation of Ni nanoparticles by the liquid phase chemical reduction method. Smaller-sized and better-dispersed Ni nanoparticles can be successfully achieved using amine-terminated generation 2 PAMAM dendrimers, which are ideal templates to synthesize and stabilize Ni nanoparticles. More importantly, the PAMAM can prevent Ni nanoparticles from oxidation and, therefore, achieve more active Ni. In the liquid phase hydrogenation *p*-nitrophenol, the as-prepared Ni nanoparticles show higher catalytic activity than that of Ni nanoparticles prepared in the absence of the PAMAM dendrimers, which is attributed a combination effect of the smaller size, more active Ni and better dispersion. When the weigh ratio of PAMAM to $Ni^{2+}$ is 15%, the Ni nanoparticles exhibit the best catalytic activity. The above results hint that other higher generation amine-terminated PAMAM dendrimers can be applied for the formation of Ni nanoparticles for catalyst applications. Further work along this line is being pursued.

## ACKNOWLEDGEMENT

The work was supported by the National Natural Science Foundation of China (50702025), Natural Science Foundation of the Jiangsu Higher Education Institutions of China (08KJB430009), Natural Science Foundation of Jiangsu Province (BK2009473), Foundetion of State Key Laboratory of Materials-Oriented Chemical Engineering (KL09-13) and Start up Foundation for Advanced Talents of Nanjing Normal University (2008103XGQ0051).

## REFERENCES

1. R. V. Chaudhari, S. S. Divekar, M. J. Vaidya and C. V. Rode, Single step process for the preparation of p-aminophenol, US6028227, US (2000).
2. L. T. Lee, M. H. Chen and C. N. Yao, Process for manufacturing *p*-aminophenol, US4885389, US (1998).
3. C. V. Rode, M. J. Vaidya, R. Jaganathan and R. V. Chaudhari, *Chem. Eng. Sci.*, **56**, 1299 (2001).
4. M. J. Vaidya, S. M. Kulkarni and R. V. Chaudhari, *Org. Process Res. Dev.*, **7**, 202 (2003).
5. R. Z. Chen, Y. Du, C. L. Chen, W. H. Xing, N. P. Xu, C. X. Chen and Z. L. Zhang, *J. Chem. Ind. Eng. (Chinese)*, **54**, 704 (2003).
6. Y. Du, H. L. Chen, R. Z. Chen and N. P. Xu, *Appl. Catal., A: Gen.*, **277**, 259 (2004).
7. Y. Du, H. L. Chen, R. Z. Chen and N. P. Xu, *Chem. Eng. J.*, **125**, 9 (2006).
8. R. Z. Chen, Q. Q. Wang, Y. Du, W. H. Xing and N. P. Xu, *Chem. Eng. J.*, **145**, 371 (2009).
9. H. H. Lu, H. B. Yin, Y. M. Liu, T. S. Jiang and L. B. Yu, *Catal. Commun.*, **10**, 313 (2008).
10. Z. Y. Ma, L. X. Zhang, R. Z. Chen, W. H. Xing and N. P. Xu, *Chem. Eng. J.*, **138**, 517 (2008).
11. H. G. Zheng, J. H. Liang, J. H. Zeng and Y. T. Qian, *Mater. Res. Bull.*, **36**, 947 (2001).
12. A. Nandi, M. D. Gupta and A. K. Banthia, *Mater. Lett.*, **52**, 203 (2002).
13. Y. Houa and S. Gao, *J. Mater. Chem.*, **13**, 1510 (2003).
14. K.Yu, D. J. Kim, H. S. Chung and H. Liang, *Mater. Lett.*, **57**, 3992 (2003).
15. A. L. Wang, H. B. Yin, H. H. Lu, J. J. Xue, M. Ren and T. S. Jiang, *Langmuir*, **25**, 12736 (2009).
16. R. Esfand and D. A. Tomalia, *Drug Discovery Today*, **6**, 427 (2001).
17. S. E. Stiriba, H. Frey and R. Haag, *Angew. Chem. Int. Ed.*, **41**, 1329 (2002).
18. B. J. Auten, B. P. Hahn, G. Vijayaraghavan, K. J. Stevenson and B. D. Chandler, *J. Phys. Chem. C*, **112**, 5365 (2008).
19. Y. J. Jiang and Q. M. Gao, *J. Am. Chem. Soc.*, **128**, 716 (2006).
20. M. R. Knecht, J. C. Garcia-Martinez and R. M. Crooks, *Langmuir*, **21**, 11981 (2005).
21. J. P. K. Reynhardt, Y. Yang, A. Sayari and H. Alper, *Chem. Mater.*, **16**, 4095 (2004).
22. T. R. Hendricks, E. E. Dams, S. T. Wensing and I. Lee, *Langmuir*, **23**, 7404 (2007).
23. A. Rar, J. N. Zhou, W. J. Liu, J. A. Barnard, A. Bennett and S. C. Street, *Appl. Surf. Sci.*, **175**, 134 (2001).
24. M. R. Knecht, J. C. Garcia-Martinez and R. M. Crooks, *Chem.*

*Mater.*, **18**, 5039 (2006).
25. D. A. Tomalia, H. Baker, J. R. Dewald, M. J. Hall, G. Kallos, S. J. Martin, J. Roeck, J. Ryder and P. Smith, *Polym. J. (Japan)*, **17**, 117 (1985).
26. J. Desilvestro and D. A. Corrigan, *J. Electrochem. Soc.*, **135**, 885 (1988).
27. Z. L. Liu, X. D. Wang, H. Y. Wu and C. X. Li, *J. Colloid Interf. Sci.*, **287**, 604 (2005).